Article

Polymers and Polymer Composites

Polymers and Polymer Composites
2020, Vol. 28(5) 348–355

DOI: 10.1177/0967391119879009
journals.sagepub.com/home/ppc
SAGE

Synthesis of self-healing polyurethane and its application in graphene/SnO_2-pillared carbon anode materials

Young Joon Kwon[1], Jeevan Kumar Reddy Modigunta[2], AM Shanmugharaj[3], Hyung Jin Mun[1] and Sung Hun Ryu[1]

Abstract

Self-healing polyurethane (SHPU) containing disulfide was synthesized and used as a binder to investigate its effect on the performance of reduced graphene oxide–tin oxide electrodes compared to those of polyurethane (PU) and poly(-vinylidene difluoride) (PVDF) binders in Li-ion battery (LIB). Structural and morphological characterization of the SHPU and electrode was performed using a tensile tester, Fourier transform infrared spectroscopy, X-ray diffractometer, and scanning electron microscopy. Electrochemical performance was investigated using Galvanostatic charge–discharge and electrochemical impedance measurements. The tensile properties and scanning electron microscopy photographs confirmed the self-healing characteristics of the synthesized SHPU. Electrochemical studies were conducted using an RGO-SnO_2 electrode. The electrochemical measurements revealed that the SnO_2-pillared carbon-based anode materials with SHPU binder showed improved cycling performances with an excellent reversible capacity retention compared to PU or PVDF. After 1000 cycles at 1C, the surface morphology of the electrode with SHPU showed no cracks or dendrites, while the PVDF-based electrode possessed some cracks and dendrites on its surface. The electrochemical results confirmed that SHPU binder improves the electrochemical performance of LIBs.

Keywords

Self-healing, polyurethane, binder, anode material, electrochemical property

Received 17 April 2019; accepted 5 September 2019

Introduction

Electrodes are crucial components for the overall performance of lithium-ion batteries (LIBs), where graphite is used as a standard anode material.[1–3] The demand for higher energy density LIBs is increasing in many applications, such as automobiles, and group IV elements have received much interest for this purpose. However, the use of these elements is limited due to the large volumetric change (ca. 300%) that occurs during long-term charge–discharge cycling and results in undesirable rapid capacity fading, low initial coulombic efficiency, and poor rate performance.[4,5] A continuous large volume change in the lithiation–delithiation process results in disintegration and pulverization of the electrode.[6–8]

Among the various approaches employed to avoid this limitation, chemically modified graphene and SnO_2 have been hybridized to accommodate the volume change and improve the capacity and cycling stability of the electrode material.[9–11] A pomegranate structure, where single nanoscale silicones are encapsulated by a carbon layer, has been proposed and resulted in excellent cyclability and electrode–electrolyte contact area.[12–16] SnO_2 is believed to be a promising material due to its high theoretical lithium storage capacity, low cost, and safe working potential. However, large volume changes during charge–discharge cycling hinder the practical application of SnO_2. Hybridization of SnO_2 with carbonaceous materials has

[1] Department of Chemical Engineering, Kyung Hee University, Yongin-Si, Kyunggido, South Korea
[2] Department of Chemistry and Nanoscience and Nanoengineering, Inje University, Gimhae-Si, Gyeongsangnam-do, South Korea
[3] Department of Chemistry and Centre for Energy and Alternative Fuels, Vels Institute of Science Technology and Advanced Studies (VISTAS), Chennai, Tamil Nadu, India

Corresponding author:
Sung Hun Ryu, Department of Chemical Engineering, Kyung Hee University, Yongin-Si, Kyunggido 17104, South Korea.
Email: shryu@khu.ac.kr

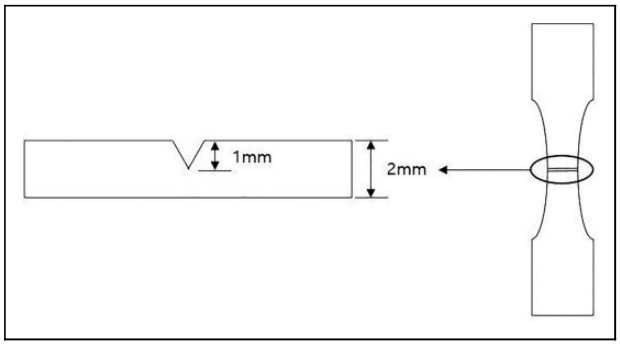

Figure 1. Schematic diagram of a tensile specimen.

been used to circumvent this limitation.[17–19] In particular, graphene has been used in hybridization because of its excellent electronic conductivity and high surface area. In situ synthesis approaches have been applied to obtain a homogeneous distribution of Sn nanoparticles in graphene sheets.[20] Jeevan Kumar Reddy et al. studied hybridization of SnO_2 with long-chain alkylamine-grafted graphene oxide, and the specific capacities decreased with increasing alkylamine chain length.[21]

Self-healing polymers can spontaneously repair mechanical damage, and this characteristic enhances the lifetime of energy storage materials.[22–26] Wang et al. used a self-healing polymer as a binder and attained a 10 times longer life cycle.[3] Multiple network binder, poly(acrylic acid)-poly(2-hydroxyethyl acrylate-co-dopamine methacrylate), with rigid-soft bonds showed self-healing behavior and improved the rate of performance of LIB.[24] Feng et al. reported the self-healing behavior of polyurethane (PU)-based on the Diels–Alder reaction and thermal movement of molecular chains.[25]

In the present study, we attempted to synthesize SnO_2-nanopillared carbon structures using dodecylamine-grafted graphene oxide as a template. A PU-based self-healing polymer was synthesized and applied to LIBs as a binder for fabrication of electrodes. The effect of the self-healing characteristic on the performance of LIBs was evaluated and compared to that of PU or commercial poly(vinylidene difluoride) (PVDF) binders.

Experiment

SnO_2-pillared dodecylamine-grafted graphene oxide (SnO_2-GN) was prepared, as previously reported.[21,27,28]

Self-healing polyurethane (SHPU) was synthesized using polycaprolactone diol (Capa™ Thermoplastics) with a molecular weight of ca. 900, 4,4′-methylenebis(phenyl isocyanate) (Sigma-Aldrich, St. Louis, MO, USA), and *p*-amino phenyl disulfide (Sigma-Aldrich). To obtain the prepolymer, a reaction between polycaprolactone diol and 4,4′-methylenebis(phenyl isocyanate) at a ratio of 8:2 was carried out at 80°C in a three-necked flask under N_2 atmosphere for 1 h. Then, 5 wt% *p*-amino phenyl disulfide was combined with 10 ml of tetrahydrofuran (THF) solvent and added to the prepolymer under stirring for 2 min to obtain SHPU.[16] The sample was held at 60°C in a vacuum oven for 16 h to remove the solvent traces (THF). For comparison, PU was synthesized as SHPU without *p*-amino phenyl disulfide.

To investigate the self-healing characteristics of SHPU, tensile stress tests (ASTM D638) were performed using a universal tensile tester (LF Plus, Lloyd Instruments) at room temperature with a crosshead speed of 5 mm min^{-1}. The tensile specimen with a thickness of 2 mm was created from the sheet prepared at 150°C using a hot press. The center of the tensile specimens was cut to a depth of 1 mm, as shown in Figure 1, and the specimens were placed in an oven at 70°C for a predetermined period of time (1, 3, or 7 days). Field Emission (FE)-scanning electron microscopy (SEM) was used to observe the change of the cut area over time.

The electrochemical performances of SnO_2-GN were measured by fabricating 2032 type coin cells using Li metal as a reference electrode. Electrodes were prepared by casting a slurry with a composition of 80 wt% active material, 10 wt% conductive agent (super P, TIMCAL, Switzerland), and 10 wt% SHPU or PVDF (Kureha KF100) (for the reference sample) onto copper foil. The slurry was prepared by grinding the mixture in the presence of *N*-methyl pyrrolidone solvent using a mortar for 15 min. The viscous slurry coated onto copper foil was dried in an oven at 100°C for 5 h. The electrode was assembled into a 2032 type coin type cell with a 1 M $LiPF_6$ solution in a 1:1 (volume) mixture of ethylene carbonate and diethyl carbonate (Merck Co., USA). The electrochemical properties were evaluated by galvanostatic charge and discharge measurements in the voltage range of 0.1–2.0 V versus Li/Li^+ using a battery analyzer (WonATech, Korea). Cyclic voltammetry curves were obtained at a scan rate of 0.1 mV s^{-1} within the range of 0.1–1.25 V using an electrochemical work station (VersaSTAT 3 Electrochemical System). Electrochemical impedance studies were performed using an electrochemical work station (VersaSTAT 3 Electrochemical System, Ametek, USA) at an amplitude of 5.0 mV in the range of 100 kHz to 0.01 Hz.

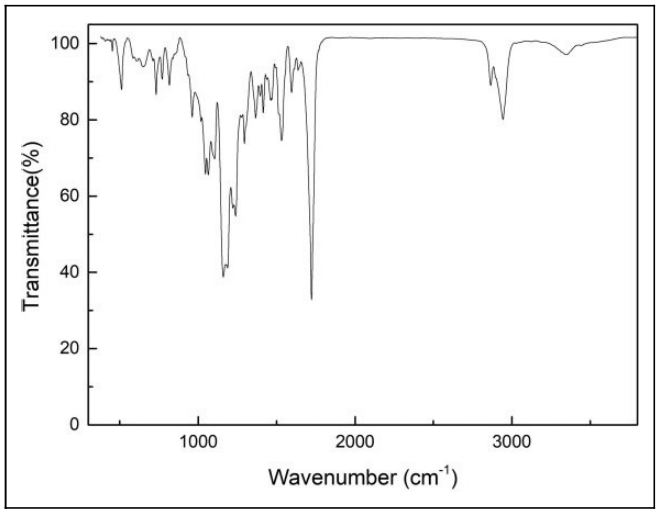

Figure 2. FTIR spectrum of the synthesized self-healing polyurethane.
FTIR: Fourier transform infrared spectroscopy.

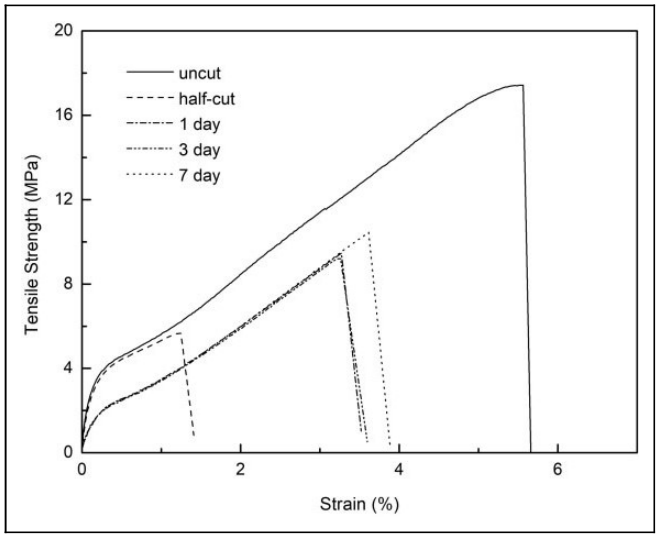

Figure 3. Tensile stress–strain data of SHPU under various treatment periods at 70°C.
SHPU: self-healing polyurethane.

Results and discussion

The Fourier transform infrared spectroscopy analysis results of the synthesized SHPU are shown in Figure 2. The peaks at 2865 and 2943 cm^{-1} represent –CH asymmetric stretching, and the peak at 1722 cm^{-1} belongs to C=O of the carboxylic group. The C=O in amide is overlapped with the carboxylic peak at ca. 1630–1680 cm^{-1}. The peak at 511 cm^{-1} is attributed to the S–S bond, which induces the self-healing behavior of SHPU.

The tensile properties of the half-cut SHPU specimens are shown in Figure 3. The tensile strength and elongation of the half-cut specimen were less than 30% of that of the original uncut specimen. The tensile properties of PU and SHPU without half-cut are similar. The tensile strength and elongation of half-cut SHPU held at 70°C for 1 day increase by 68% and 150%, respectively, and they further increase by 84% and 190% after treatment for 7 days compared to the half-cut specimen. These significant increases of tensile strength and elongation are attributed to the self-healing behavior of SHPU. It has been reported that the disulfide group is responsible for the self-healing property.[29,30] SEM photographs of specimens are shown in Figure 4 and clearly show that the cut area becomes narrower with increasing time and eventually it is fully healed. These photographs support the notion that the improvement of tensile properties shown in Figure 3 is dependent on the self-healing capability of SHPU.

The electrochemical properties of the SnO_2-GN-PU, SnO_2-GN-SHPU, and SnO_2-GN-PVDF anodes in lithium-ion half-cells are evaluated with respect to constant current charge–discharge cycling in the potential range of 0.1–2.0 V. The charge–discharge profiles of SnO_2-GN-SHPU and SnO_2-GN-PVDF at the 1st, 100th, and 1000th cycles measured at a 2C rate are shown in Figure 5. The first cycle discharge and charge capacities of SnO_2-GN-PU and

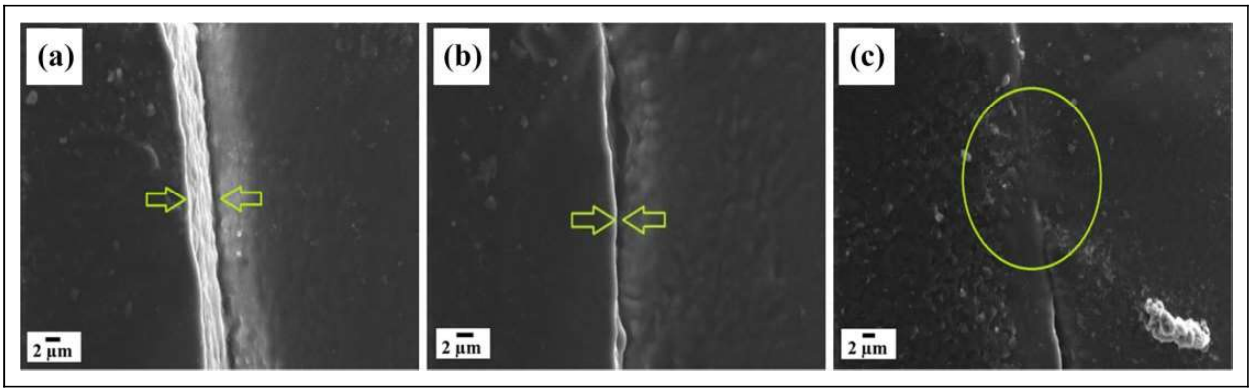

Figure 4. (a)–(c). FE-SEM photographs of half-cut specimens of SHPU after various treatment periods.
SHPU: self-healing polyurethane; SEM: scanning electron microscope.

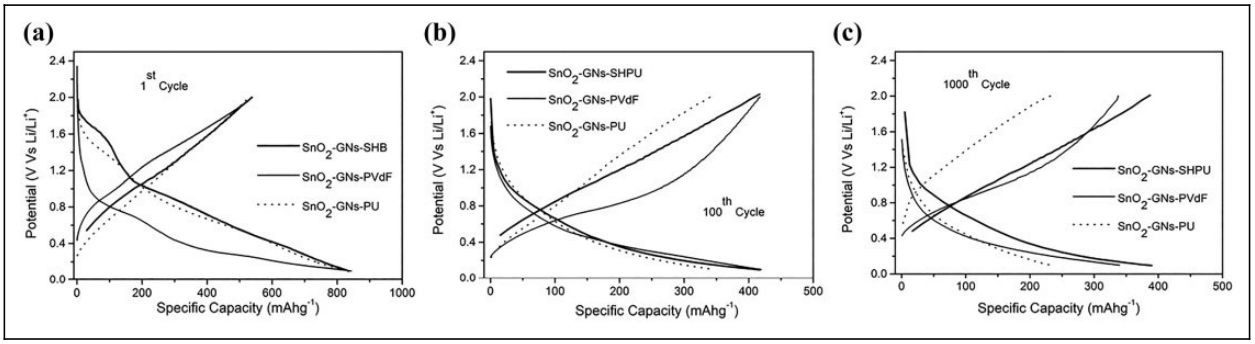

Figure 5. Charge–discharge profiles of SnO_2-GN-PU, SnO_2-GN-SHPU, and SnO_2-GN-PVDF at (a) 1st cycle, (b) 100th cycle, and (c) 1000th cycle.

SnO_2-GN-SHPU are observed to be 835/530 and 836/537 mA hg^{-1} with first columbic efficiencies of 63.5% and 64%, respectively. Similarly, the first discharge and charge capacities of SnO_2-GN-PVDF are observed to be 843 and 539 mA hg^{-1}, respectively, with a columbic efficiency of 64%. However, as cycling proceeded to the 100th cycle, the discharge and charge capacities became 346/342 and 417/416 mA hg^{-1}, respectively, with columbic efficiencies of ca. 100% for SnO_2-GN-PU and SnO_2-GN-SHPU. For SnO_2-GN-PVDF, the discharge and charge capacities are 419 and 417 mA hg^{-1}, respectively, with a columbic efficiency of 100%. At the end of the 1000th cycle, the discharge and charge capacities are 233/232 and 389/387 mA hg^{-1} with columbic efficiencies of ca. 100% for SnO_2-GN-PU and SnO_2-GN-SHPU, respectively, while SnO_2-GN-PVDF shows discharge and charge capacities of 339 and 337 mA hg^{-1}. The capacity retention of SnO_2-GN-SHPU (72%) is much higher than that of SnO_2-GN-PU (44%) from the 1st to 1000th cycle and even higher than that of SnO_2-GN-PVDF (62%), as shown in Figure 6. It has been reported that avoiding cracking and pulverization of the electrode can result in enhanced cycling stability.[23–25] Thus, the constant cycling performance with excellent capacity retention of SnO_2-GN-SHPU can be attributed to the self-healing nature of the SHPU binder.

The specific capacities of SnO_2-GN-SHPU and SnO_2-GN-PVDF are evaluated at various current rates, and the results are shown in Figure 7. The specific capacity decreases with increasing current rate for both SHPU and PVDF. However, the relative decay of specific capacity for SHPU is relatively less than that of PVDF. When the C-rate returns to the initial 0.5C rate at the 50th cycle, SnO_2-GN-SHPU and SnO_2-GN-PVDF recover up to 90% and 86% of their initial specific capacity values, respectively. This supports better reversibility and cyclability of SnO_2-GN-SHPU compared to SnO_2-GN-PVDF.

Electrochemical impedance spectroscopy (EIS) of SnO_2-GN-SHPU and SnO_2-GN-PVDF is performed to understand the interfacial electrochemistry and reaction mechanism in the frequency range of 100 kHz–0.01 Hz. Typical Nyquist plots of the AC impedance before and after cycling are shown in Figure 8(a) and (b). In general, the impedance spectrum consists of a depressed arc followed by a straight line inclined at 45° angle. The equivalent circuit adopted for calculations is shown in Figure 8(c). R_e represents the internal ohmic resistance, which involves the resistance of the electrolyte and other resistive components, corresponding to the intercept of the plots with the real axis (Z_{re}) at high frequency. R_f and C_{dl1} corresponding to the semicircle in the high-frequency region represent the resistance and capacitance of solid electrolyte interface (SEI) films. R_{ct} and C_{dl2} related to the semicircle at medium to low frequencies correspond to the charge transfer

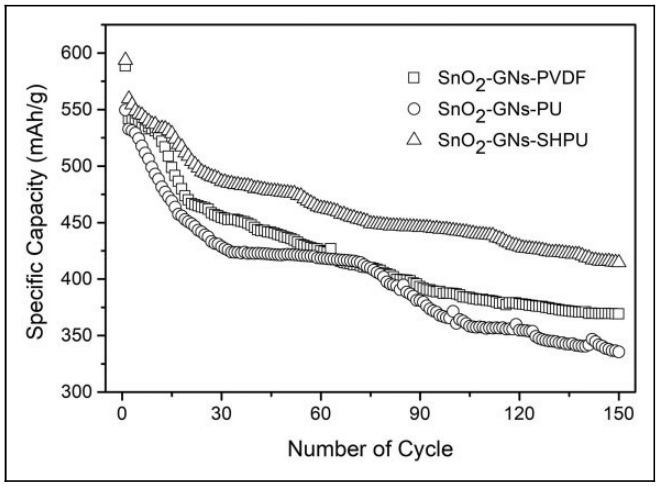

Figure 6. Comparison of the capacity retention of SnO_2-GN-PU, SnO_2-GN-SHPU, and SnO_2-GN-PVDF.
SnO_2-GN: SnO_2-pillared dodecylamine-grafted graphene oxide; PVDF: poly(vinylidene difluoride); SHPU: self-healing polyurethane; PU: polyurethane.

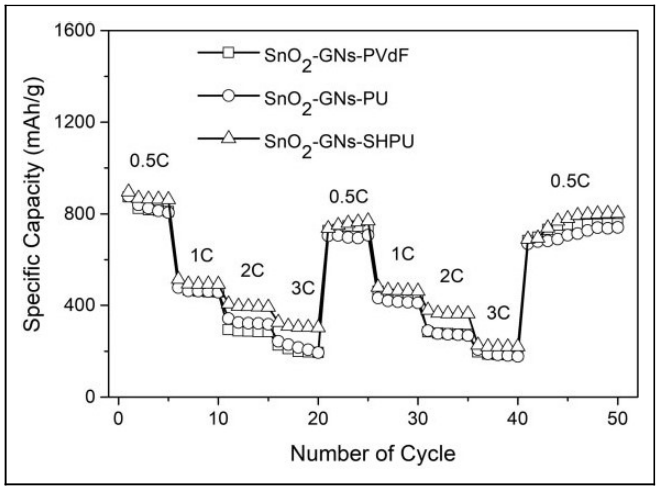

Figure 7. Electrochemical impedance spectroscopy (EIS) results of SnO_2-GN-PU, SnO_2-GN-SHPU, and SnO_2-GN-PVDF.
SnO_2-GN: SnO_2-pillared dodecylamine-grafted graphene oxide; PVDF: poly(vinylidene difluoride); SHPU: self-healing polyurethane; PU: polyurethane.

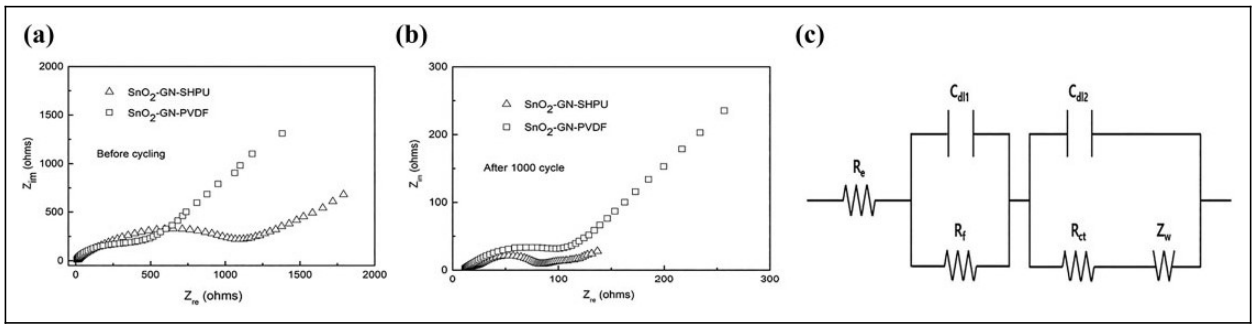

Figure 8. Specific capacity of SnO_2-GN-SHPU and SnO_2-GN-PVDF at various current rates.
SnO_2-GN: SnO_2-pillared dodecylamine-grafted graphene oxide; PVDF: poly(vinylidene difluoride); SHPU: self-healing polyurethane.

resistance and capacitance, respectively. The Warburg impedance, Z_W, refers to the sloping region at low frequencies and is directly associated with the lithium-ion diffusion process in the electrode. The values of R_e, R_f, R_{ct}, and R_{total} are listed in Table 1. The resistance values for SnO_2-GNs-SHPU and SnO_2-GNs-PVDF are quite different as the EIS resembles the surface nature of the electrode material present in the cell. Due to SEI formation after cell fabrication, the R_{ct} value is

Table 1. Values of R_e, R_f, R_{ct}, and R_{total}.

	SnO_2-GNs-SHPU	SnO_2-GNs-PVDF
R_e (Ω)	15.6	14.6
R_f (Ω)	94.63	68.5
R_{ct} (Ω)	493.8	181.4
R_{total}(Ω)	604.04	264.54
i_0 ($\times 10^{-5}$ A)	5.23	14.3

SnO_2-GN: SnO_2-pillared dodecylamine-grafted graphene oxide; PVDF: poly(vinylidene difluoride).

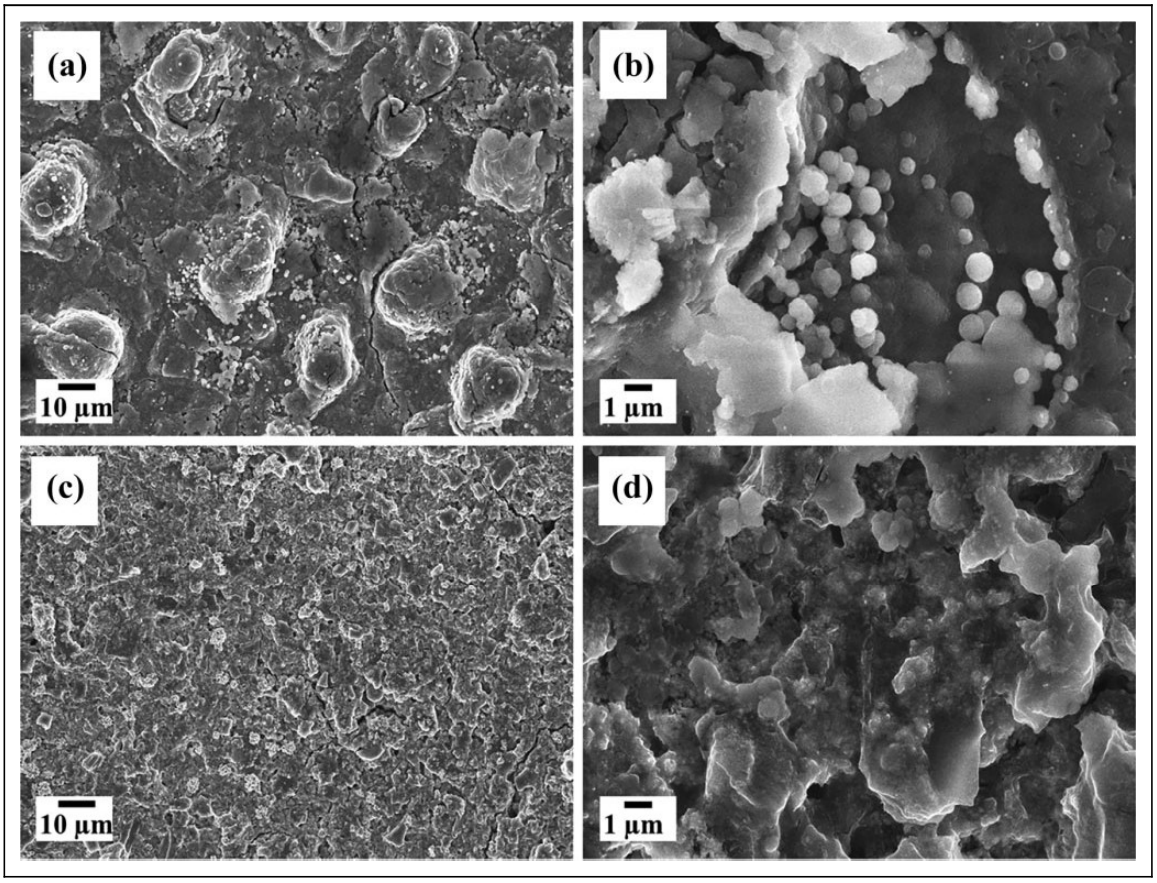

Figure 9. Surface morphologies of (a, b) SnO_2-GN-PVDF and (c, d) SnO_2-GN-SHPU electrodes after 1000 cycles.
SnO_2-GN: SnO_2-pillared dodecylamine-grafted graphene oxide; PVDF: poly(vinylidene difluoride); SHPU: self-healing polyurethane.

higher for the SHPU-based electrode and lower for the PVDF-based electrode. The higher initial solution resistance (R_s) and R_{ct} of the SHPU-based electrode can be attributed to the surface roughness of the electrode. This is further corroborated by the exchange current density (i_0), which is calculated using $i_0 = RT/nFR_{ct}$, where R is the gas constant, T is the absolute temperature, n is the number of electrons, F is the Faraday constant, and R_{ct} is the charge-transfer resistance. Relatively, the value of the exchange current density (i_0) for SnO_2-GN-PVDF at its initial cycle performance is higher than that of the SnO_2-GN-SHPU-based electrode system.

To better understand the performance of SHPU as an efficient binder at a higher current rate of 1C, the surface morphologies of the electrodes after 1000 cycles are examined, and the FE-SEM photographs are shown in Figure 9. Figure 9(a) and (b) corresponds to electrodes prepared using PVDF. These photographs show cracks on the surface and dendrites due to the side reaction on the electrode materials during the charge–discharge process. Dendrites are formed due to the surface and interfacial reaction between the electrode surface and components in the electrolyte.[31] However, in the case of Figure 9(c) and (d), which are prepared using SHPU as a binder, the photographs show a normal surface without any cracks or dendrites. This indicates that most of the surface cracks formed by the charge–discharge process were healed, which can be attributed to the self-healing characteristic of the SHPU binder. Although the exact self-healing mechanism during charge–discharge process is under investigation, this surface morphology study also supports the improved electrochemical performances of SnO_2-GNs-SHPU compared to SnO_2-GNs-PVdF.

Conclusion

Polyurethane-based self-healing polymer (SHPU) was prepared successfully using polycaprolactone diol and 4,4′-methylenebis(phenyl isocyanate) as starting materials followed by the self-healing additive, *p*-amino phenyl disulfide. SHPU was subjected to different characterization methods to confirm the formation and evaluate its properties. SHPU was tested to gain better understanding of its capability as a binder in the application of LIBs, namely for the case of SnO_2-pillared carbon anodes. Electrochemical measurements revealed that the SnO_2-pillared carbon-based anode materials with self-healing binder had relatively better cycling performances with excellent reversible capacity relative to the electrode prepared from commercial PU or PVDF binder-based anode materials at a 1C rate over extended cycling. Based on the electrochemical and physical characterizations, SHPU can be a good future binder for applications in LIB anode materials.

Authors contribution

The authors YJK and JKRM have equally contributed to this manuscript.

Declaration of conflicting interests

The authors declared no potential conflicts of interest with respect to the research, authorship, and/or publication of this article.

Funding

The authors received no financial support for the research, authorship, and/or publication of this article.

ORCID iD

Sung Hun Ryu https://orcid.org/0000-0001-8593-6737

References

1. Buqa H, Goers D, Holzapfel M, et al. High rate capability of graphite negative electrodes for lithium-ion batteries. *J Electrochem Soc* 2005; 152: A474–A481.
2. Urban MW. Dynamic materials: the chemistry of self-healing. *Nat Chem* 2012; 4: 80–82.
3. Wang C, Wu H, Chen Z, et al. Self-healing chemistry enables the stable operation of silicon microparticle anodes for high-energy lithium-ion batteries. *Nat Chem* 2013; 5: 1042–1048.
4. Yang S, Zhao F, Li X, et al. Electrode structural changes and their effects on capacitance performanceduring preparation and charge-discharge processes. *J Energy Storage* 2019; 24: 100799.
5. Mukai SR, Hasegawa T, Takagi M, et al. Reduction of irreversible capacities of amorphous carbon materials for lithium ion battery anodes by Li_2CO_3 addition. *Carbon* 2004, 42: 837–842.
6. Basu S, Koratkar N and Shi Y. Structural transformation and embrittlement during lithiation anddelithiation cycles in an amorphous silicon electrode. *Acta Materialia* 2019; 175: 11–20.
7. Armand M and Tarascon JM. Building better batteries. *Nature* 2008; 451: 652–657.
8. Cao K, Li P, Zhang Y, et al. In situ TEM investigation on ultrafast reversible lithiation and delithiationcycling of Sn@C yolk-shell nanoparticles as anodes for lithium ion batteries. *Nano Energy* 2017; 40: 187–194.
9. He Y, Li A, Dong C, et al. Mesoporous tin-based oxide nanospheres/reduced graphene composites as advanced anodes for lithium-ion half/full cells and sodium-ion batteries, *Chem Eur J* 2017; 23: 13724–13733.
10. Wang H, Cui LF, Yang Y, et al. Mn_3O_4−graphene hybrid as a high-capacity anode material for lithium ion batteries. *J Am Chem Soc* 2010; 132: 13978–13980.
11. Paek SM, Yoo E and Honma I. Enhanced cyclic performance and lithium storage capacity of sno_2/graphene nanoporous electrodes with three-dimensionally delaminated flexible structure. *Nano Lett* 2009; 9: 72–75.
12. Liu N, Lu Z, Zhao J, et al. A pomegranate-inspired nanoscale design for large-volume-change lithium battery anodes. *Nature Nanotechnol* 2014; 9: 187–192.
13. Chan CK, Peng HL, Liu G, et al. High-performance lithium battery anodes using silicon nanowires. *Nature Nanotechnol* 2008; 3: 31–35.
14. Kovalenko I, Zdyrko B, Magasinki A, et al. A major constituent of brown algae for use in high-capacity Li-ion batteries. *Science* 2011; 334: 75–79.
15. Liu G, Xun S, Vukmirovic N, et al. Polymers with tailored electronic structure for high capacity lithium battery electrodes. *Adv Mater* 2011; 23: 4679–4683.
16. Wu H and Cui Y. Designing nanostructured Si anodes for high energy lithium ion batteries. *Nano Today* 2012; 7: 414–429.
17. Chang CC, Liu SJ, Wu JJ, et al. Nano-tin oxide/tin particles on a graphite surface as an anode material for lithium-ion batteries. *J Phys Chem* 2007; C111: 16423–16427.
18. Fu Y, Ma R, Shu Y, et al. Preparation and characterization of SnO_2/carbon nanotube composite for lithium ion battery applications. *Mater Lett* 2009; 63: 1946–1948.

19. Zhu X, Zhu Y, Murali S, et al. Reduced graphene oxide/tin oxide composite as an enhanced anode material for lithium ion batteries prepared by homogenous coprecipitation. *J Power Sources* 2011; 196: 6473–6477.
20. Wang G, Wang B, Wang X, et al. Sn/graphene nanocomposite with 3D architecture for enhanced reversible lithium storage in lithium ion batteries. *J Mater Chem* 2009; 19: 8378–8384.
21. Jeevan Kumar Reddy M, Ryu SH and Shanmugharaj AM. Synthesis of SnO_2 pillared carbon using long chain alkylamine grafted graphene oxide: an efficient anode material for lithium ion batteries. *Nanoscale* 2016; 8: 471–482.
22. Benight SJ, Wang C, Tok JBH, et al. Stretchable and self-healing polymers and devices for electronic skin. *Prog Polym Sci* 2013; 38: 1961–1977.
23. Tee BCK, Wang C, Allen R, et al. An electrically and mechanically self-healing composite with pressure- and flexion-sensitive properties for electronic skin applications. *Nat Nano* 2012; 7: 825–832.
24. Xu Z, Yang J, Zhang T, et al. Silicon microparticle anodes with self-healing multiple network binder. *Joule* 2018; 2: 950–961.
25. Feng L, Yu Z, Bian Y, et al. Self-healing behavior of polyurethanes based on dual actions of thermo-reversible Diels-Alder reaction and thermal movement of molecular chains. *Polymer* 2017; 124: 48–59.
26. Luo C, Fan XL, Ma ZH, et al. Self-healing chemistry between organic material and binder for stable sodium-ion batteries. *Chem* 2017; 3: 1050–1062.
27. Shanmugharaj AM, Yoon JH, Yang WJ, et al. Synthesis, characterization, and surface wettability properties of amine functionalized graphene oxide films with varying amine chain lengths. *J Colloid Interface Sci* 2013; 401: 148–154.
28. Ryu SH and Shanmugharaj AM. Influence of long-chain alkylamine-modified graphene oxide on the crystallization, mechanical and electrical properties of isotactic polypropylene nanocomposites. *Chem Eng J* 2014; 244: 552–560.
29. Post W, Cohades A, Michaud V, et al. Healing of a glass fibre reinforced composite with a disulphide containing organic-inorganic epoxy matrix. *Compos Sci Technol* 2017; 152: 85–93.
30. Chang K, Jia H and Gu SY. A transparent, highly stretchable, self-healing polyurethane based on disulphide bonds. *Eur Polym J* 2019; 112: 822–831.
31. Harry KJ, Hallinan DT, Parkinson DY, et al. Detection of subsurface structures underneath dendrites formed on cycled lithium metal electrodes. *Nature Mater* 2013; 13: 69–73.